Parametrization of the antiproton inclusive production cross section on nuclei

R. P. Duperray, C.-Y. Huang,* K. V. Protasov, and M. Buénerd†
Laboratoire de Physique Subatomique et de Cosmologie, 53 avenue des Martyrs, 38026 Grenoble Cedex, France
(Received 14 May 2003; published 24 November 2003)

A new parametrization of the $\bar{p}$ inclusive production cross section in proton-proton and proton-nucleus collisions is proposed. A sample of consistent $pA \to \bar{p}X$ experimental data sets measured on $1 \leqslant A \leqslant 208$ nuclei, from 12 GeV up to 400 GeV incident energy, has been used to constrain the parameters. A broader energy domain is covered for the $pp \to \bar{p}X$ reaction and with a simplified functional form used in the fits. The agreement obtained with the data is good. The results are discussed.

DOI: 10.1103/PhysRevD.68.094017 PACS number(s): 13.85.Ni

I. INTRODUCTION

An accurate description of the inclusive antiproton production cross section in proton-nucleus collisions necessarily relies on the empirical approach to the experimental data since theoretical calculations can provide at best approximate values in the current stage of the theory. The aim of the present work was to develop a handy analytical parametrization for the description of the inclusive $\bar{p}$ production cross section in proton-proton (pp) and proton-nucleus (pA) collisions on the basis of the existing body of data, updating the former works on the subject.

The motivations of this work have their origin in cosmic ray (CR) physics, where a good knowledge and a good description of the $\bar{p}$ inclusive production cross section is a key requirement for a detailed understanding of the production and propagation of secondary galactic and atmospheric antiprotons. The $\bar{p}$ component of the CR flux is an important window for cosmology. The main contribution to this flux originates from the interaction of the high-energy CR flux with the interstellar matter (ISM) in the galaxy. These $\bar{p}$'s are called secondary galactic. In addition to the secondary products, a primary component could exist, arising, for example, from dark matter neutralino annihilation [1] or from the evaporation products of primordial black holes [2], both being of major physical and astrophysical interest. Such signatures could be obtained only if the basic processes of galactic and atmospheric $\bar{p}$ production cross sections in pp and pA collisions are known with good enough accuracy over a momentum range extending from around threshold up to a few hundreds of GeV, where the CR flux becomes vanishingly small.

The approach used here closely follows the forms used by Kalinovskii, Mokhov, and Nikitin (KMN) [3] for the description of the $pA \to \bar{p}X$ cross section. The functional form used in this reference has been modified in order to reproduce a much larger sample of data sets over a much larger dynamical range and for a larger range of nuclear mass than in the original work. This work extends a previous effort covering a more limited domain of incident momentum and of nuclear mass [4,5].

II. INCLUSIVE CROSS SECTIONS IN HADRON COLLISIONS

In high-energy hadron collisions the final state is often complex, many particles being produced in the collision. The inclusive single-particle production cross section is a quantity of interest in many physics studies for a reaction $ab \to cX$, where c is the particle of interest and where X represents all the other particles produced in any quantum final state allowed in the collision. The invariant inclusive single-particle distribution is defined by

$$f(ab \to cX) = E_c \frac{d^3\sigma}{dp_c^3} = \frac{E_c}{\pi} \frac{d^2\sigma}{dp_\parallel dp_\perp^2} = \frac{d^2\sigma}{\pi dy d(p_\perp^2)}, \quad (1)$$

where $d^3\sigma/dp_c^3$ is the triple differential cross section for detecting particle c within the phase-space volume element d^3p_c. E_c is the total energy of c, while $p_\parallel$ and $p_\perp$ are the longitudinal and transverse components of $\mathbf{p}_c$, respectively. The rapidity variable $y = 0.5 \ln[(E+p_\parallel)/(E-p_\parallel)]$ is often used to describe the $p_\parallel$ dependence of the cross section because of its interesting properties in Lorentz transformations [6]. To obtain the last expression in Eq. (1), an azimuthal symmetry of the differential cross section was used. It is also convenient to introduce the following dimensionless variables:

$$x_f = \frac{p_\parallel^*}{p_{\parallel \max}^*} \text{ and } x_R = \frac{E^*}{E_{\max}^*}, \quad (2)$$

where x_f is the Feynman scaling variable and x_R the radial scaling variable (which depends only on the radial distance from the kinematic boundary [7]), with $p_\parallel^*$ and $p_{\parallel \max}^*$ being the longitudinal momentum of the particle and its maximum possible value in the center-of-mass (c.m.) frame, respectively, while similarly E^* and $E_{\max}^*$ are the total energy of the inclusive particle and its maximum possible value in the c.m. frame, respectively. The latter can be written as $E_{\max}^* = (s - M_{X,\min}^2 + m_p^2)/2\sqrt{s}$, with $M_{X,\min}^2 = 2m_p + m_A/A$ being the minimum possible mass of the recoiling particle in the considered process and $\sqrt{s}$ the total c.m. energy. Note that for

*Present address: Max Planck Institute für Kernphysik, D-69117 Heidelberg, Germany.
†Corresponding author: Email address: buenerd@lpsc.in2p3.fr

TABLE I. List of the experimental $\bar{p}$ production cross-section data included in the χ^2 minimization procedure, in increasing energy order.

Experience	Target	p_{inc} or $\sqrt{s}$ GeV/c (GeV)	$\bar{p}$ kinematic range GeV/c	θ_{lab} mrad
Sugaya *et al.* KEK-PS 1998 [17]	C, Cu, Al, Pb	12	p_{lab}: 1.0–2.5	89
Marmer *et al.* ANL 1969 [18]	Be, Cu	12.3	p_{lab}: 0.820, 1.030	0, 0.17, 10
Abbott *et al.* BNL 1993 [19]	Al	14.6	m_t: 0–0.3 y: 1.0–1.6	
Allaby *et al.* CERN 1970 [20]	p, Be, Al, Cu, Pb	19.20	p_{lab}: 4.5–18.3	12.5–70
Dekker *et al.* CERN 1965 [21]	p, Be, Pb	18.8, 23.1	p_{lab}: 4–12	0, 100
Eichten *et al.* CERN 1972 [22]	Be, Al, Cu, Pb	24	p_{lab}: 4–18	17–127
Kalmus *et al.* CERN 1971 [23]	Be	24–26	p_{lab}: 0.6–2.5	310
Snow *et al.* BNL 1985 [24]	Pt	28.4	p_{lab}: 0.606–0.730	0–0.17
Barton *et al.* FNAL 1983 [25]	p, C, Cu, Al, Ag, Pb	100	p_{lab}: 30–88 $p_\perp$: 0.3, 0.5	
Johnson *et al.* FNAL 1978 [26]	p	100, 200, 300	$p_\perp$: 0.25–1.5 $0.05<x_R<1.0$	
Baker *et al.* FNAL 1974 [27]	Be	200, 300	p_{lab}: 23–197	3.6
Cronin *et al.* FNAL 1975 [28]	Be, Ti, W	300	$p_\perp$: 0.76–6.91	77
Antreasyan *et al.* FNAL 1979 [29]	p, d, Be, Ti, W	200, 300, 400	$p_\perp$: 0.77–6.91	77
Guettler *et al.* CERN 1976 [30]	p	$23<\sqrt{s}<63$	$p_\perp$: 0.1–0.3 $x_f=0$	
Capiluppi *et al.* CERN 1974 [31]	p	$23.3<\sqrt{s}<63.7$	p_{lab}: 1.5–10	80–350

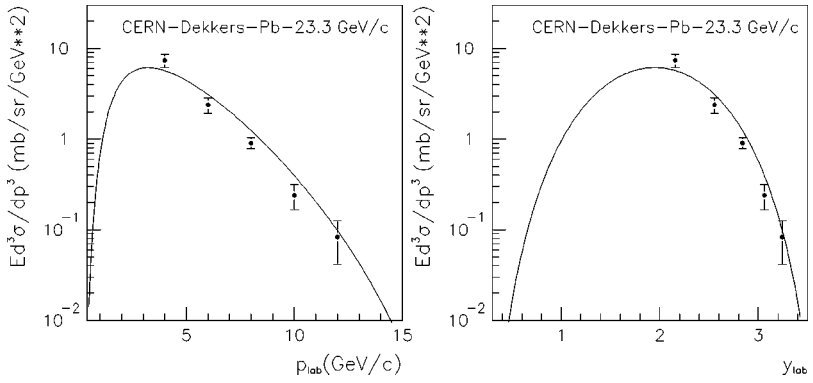

FIG. 1. Experimental $\bar{p}$ production cross section for $p+\mathrm{Pb}$ collisions at 23.1 GeV/c and at 0 degree scattering angle [21] compared with the parametrization (4), plotted against particle momentum p_{lab} (left) and rapidity y (right). In this latter case, the distribution is symmetric around the value of the c.m. rapidity $y_{\mathrm{c.m.}}=1.9$, corresponding to $p_0\sim 3.3$ GeV/c in the laboratory. The fit to the cross-section data in the upper $p>p_0$ region of the momentum region also determines the values of the cross section for $p<p_0$, where no data are available.

TABLE II. Values of the parameters of relation (4) obtained from fitting the experimental $\bar{p}$ production cross-sections list in Table I and the corresponding error following the PDG standard conventions.

Parameter	C_1	C_2	C_3	C_4	C_5
Value (error)	0.169 90(4)	10.28(13)	2.269(7)	3.707(27)	0.009 205(2)
Parameter	C_6	C_7	C_8	C_9	C_{10}
Value (error)	0.4812(14)	3.3600(2)	0.063 940(73)	−0.1824(15)	2.4850(6)

any nuclear collision, the kinematical variables used here will always be expressed in the nucleon-nucleon (NN) rather than in the nucleon-nucleus c.m. frame, since the NN c.m. frame is the relevant physical system, the incident nucleon energies being on the scale of 10 GeV while the average binding energy of the nucleon in the nucleus is about 8 MeV. Bound nucleons can be considered as free particles for the incident protons.

A parametrization of the inclusive production cross section can be guided by some general phenomenological features of hadron collisions (see [8,9] for the general physics context).

(i) All experimental hadronic production cross sections show a strong exponential decrease in transverse momentum, the exponential slope being more or less incident energy and recoil mass M_X dependent.

(ii) Hadronic scaling: The inclusive distribution $f(ab \rightarrow cX)$ of particle c is, to a good approximation, a function only of $p_\perp$ and x_f (or x_R) at the high-energy limit $\sqrt{s} \rightarrow \infty$. Furthermore, a large number of slow particles is produced (low x_f values), the distribution decreasing rapidly to zero as $x_f \rightarrow 1$, like $(1-x_f)^n$. This form can be explained by the counting rules in the parton model. These features are predicted qualitatively by the Regge poles phenomenology and the parton model.

(iii) The forward-backward symmetry of the particle production cross section is expected from first principles in nucleon-nucleon (NN) and in identical nuclei-nuclei (AA) collisions. This symmetry also holds approximately for asymmetric systems like pA or A_1A_2, in some specific dynamical range, because of the dominance of the NN collision dynamics in high-energy nuclear collisions. This is not true of course in the dynamical regions where nuclear medium effects (multiple scattering, absorption) are expected, in the target rapidity range or for light nuclei production, for example. This is true, however, in the dynamical regions governed by NN interactions, where multiple interactions or nuclear collective effects are not expected to contribute significantly, in particular for the particle production cross sections of interest here. In addition, this approximation is compatible with some experimental results for proton [10], antiproton [11,12], antideuteron [12], and pion [13] produc-

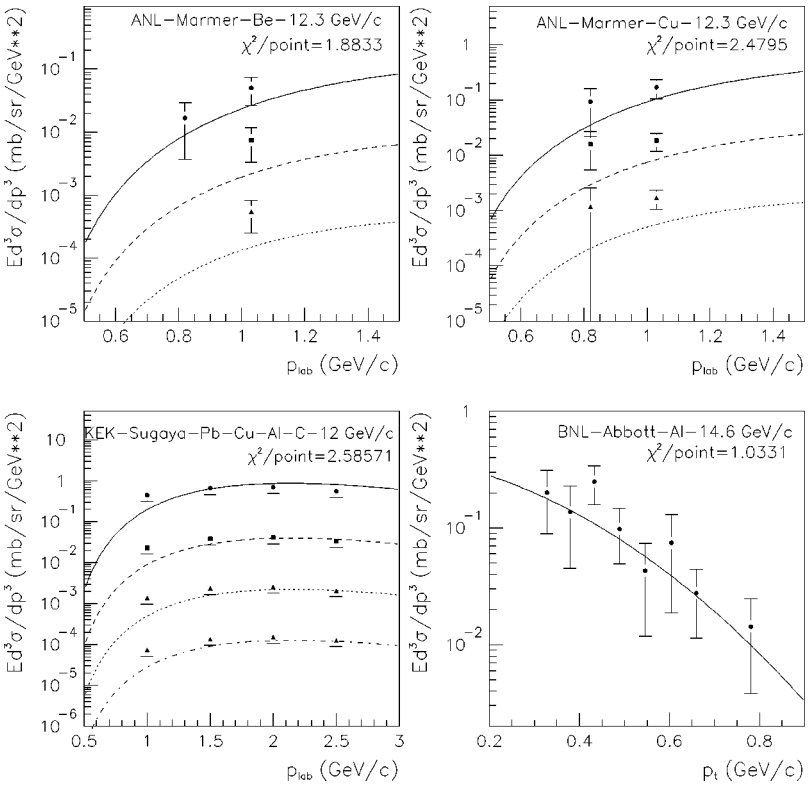

FIG. 2. Experimental data points from [17–19] compared to the best-fit calculations.

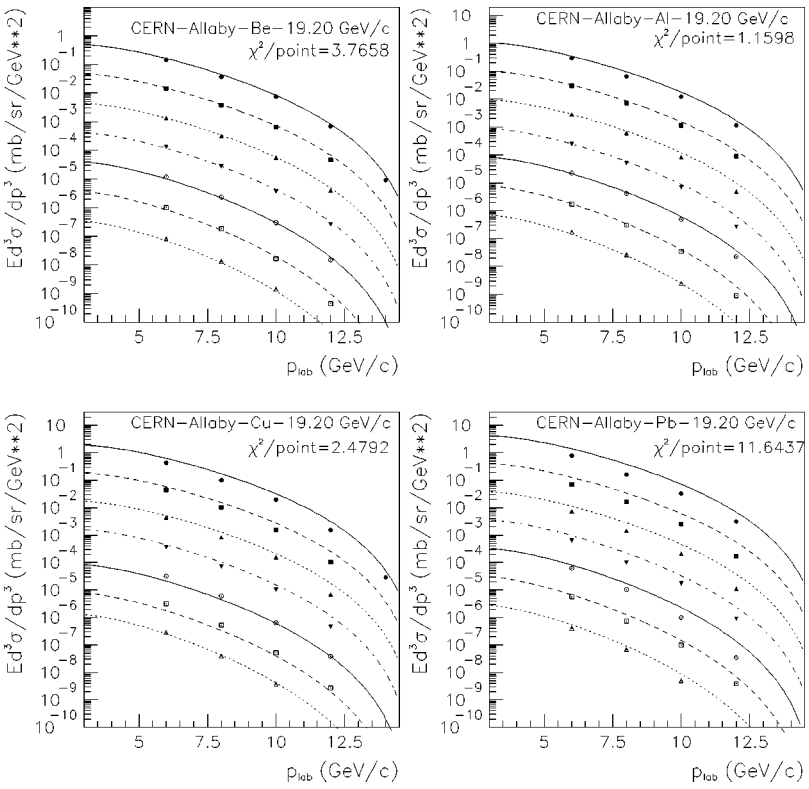

FIG. 3. Experimental data points from [20] compared to the best-fit calculations.

tions. Note also that this same argument on symmetry was used previously for $p+\mathrm{Be}$ collisions in [23] and for $p+\mathrm{Be,Al,Cu,Au}$ in [10,13], where the relation to quasifree NN collisions is also explicitly referred to. It is also supported by theoretical RQMD calculations for asymmetric nuclear collisions [14].

For NN collisions, in the central region of maximum baryon production cross section, where the c.m. rapidity $y^*=0$, the inclusive distribution consists of a plateau which width increases slowly with the incident energy. This plateau reduces to a simple maximum over the energy range considered here. The inclusive distribution rises again in the frag-

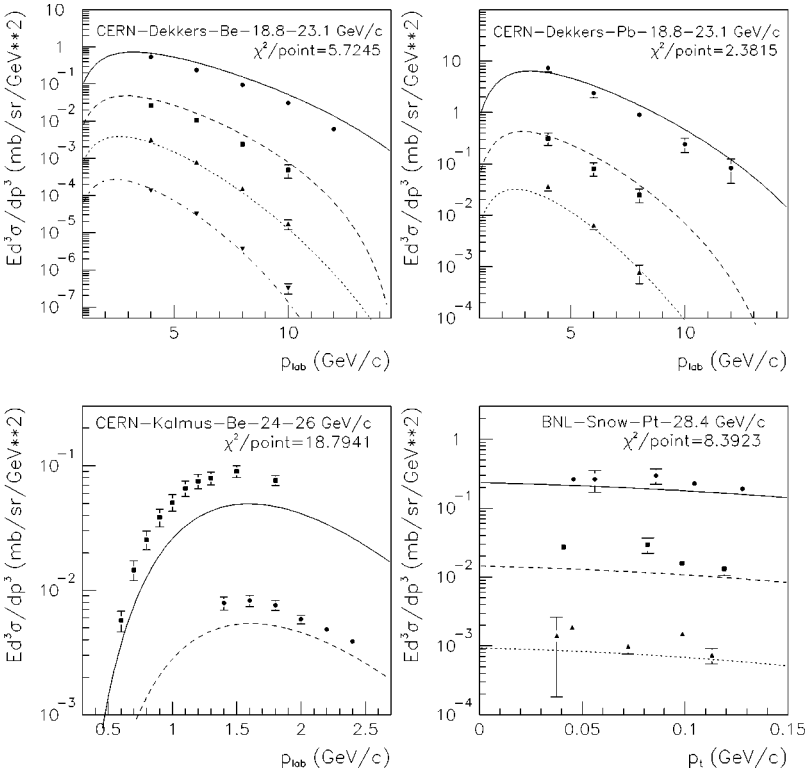

FIG. 4. Experimental data points from [21,23,24] compared to the best-fit calculations.

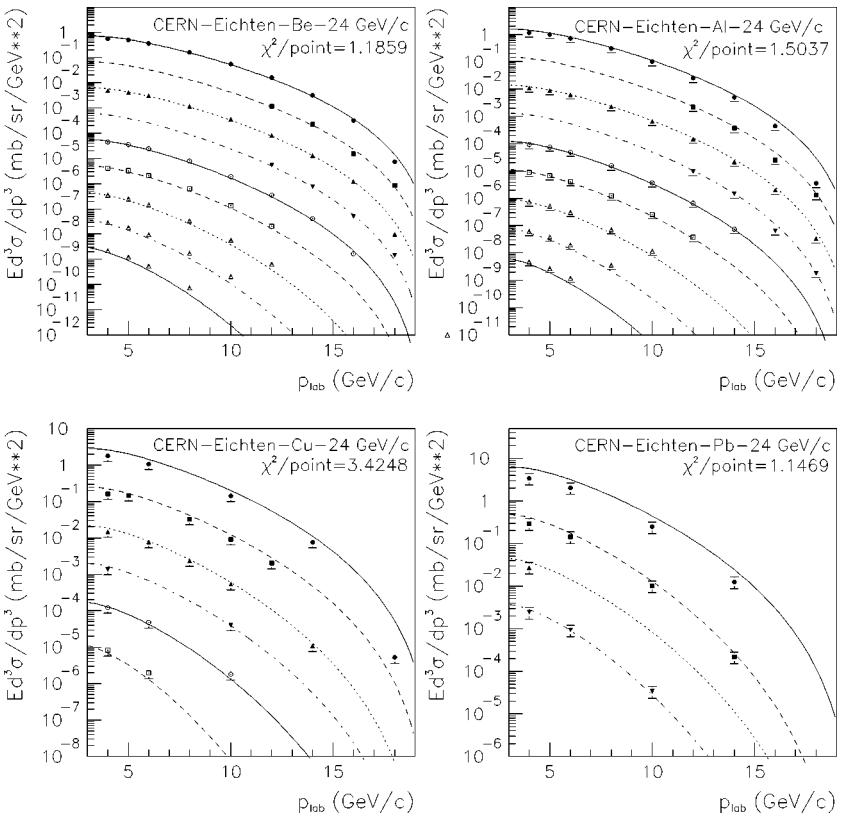

FIG. 5. Experimental data points from [22] compared to the best-fit calculations.

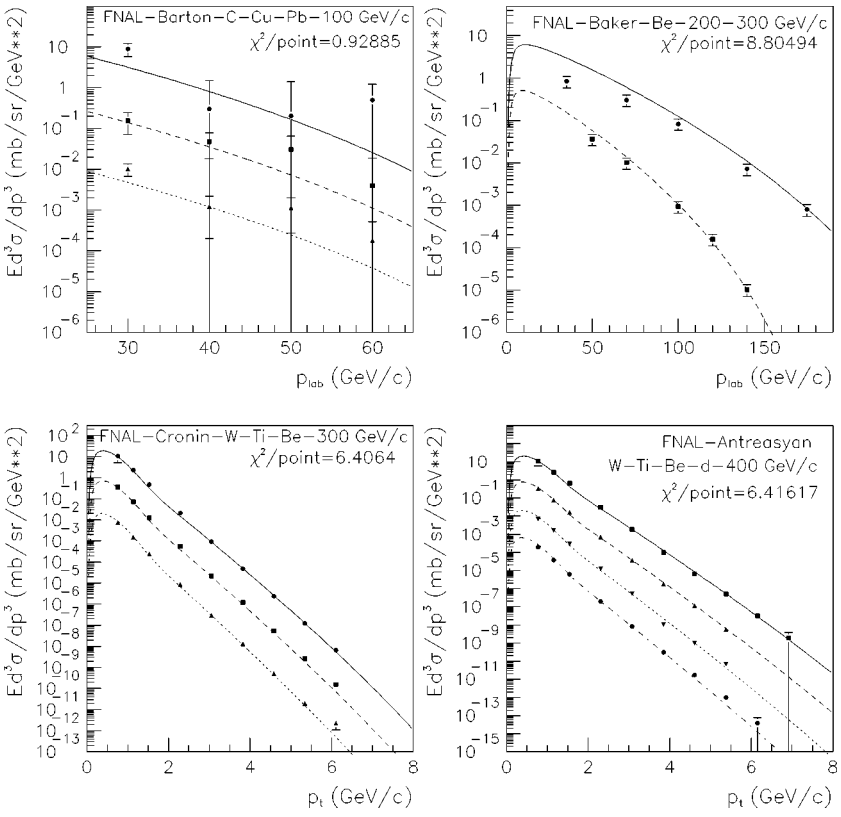

FIG. 6. Experimental data points from [25,27–29] compared to the best-fit calculations.

TABLE III. Comparison between this work and the other parametrizations.

System	Parametrization	χ^2 per point
pp,pA	KMN [3]	80.0
pp,pA	this work (4)	5.3
pp	Tan and Ng [36]	28.1
pp	this work (6)	3.6

mentation region where $y^* \rightarrow \pm y^*_{\max}$ for particles which can be produced diffractively, but this is not the case for $\bar{p}$ and the inclusive distribution is expected to drop to zero in the fragmentation region. Although some weak x_f dependence has been observed for the nuclear mass term in [25], it was contradicted for antiprotons in [24], and it has been neglected here.

This approximate symmetry property is extremely useful in the description of the antiproton data, and potentially of other particle production, since it may extend significantly the range of validity of the analytical fit to the data, as discussed below.

III. PARAMETRIZATION OF THE $p+A \rightarrow \bar{p}+X$ CROSS SECTION

Following the approach proposed in [3], the former phenomenological features of hadron collisions have been used to constrain the parameters of a functional form describing the inclusive $\bar{p}$ production cross section, which could reproduce all the relevant experimental data available from *pp* and *pA* collisions. The data used are listed in Table I. The measurements on nuclear targets cover basically the whole range of nuclear mass, from proton to lead, over a range of incident energies from 12 GeV up to 400 GeV, matching the useful range for CR studies.

The KMN parametrization used previously [3] is in very poor agreement with the data listed in Table I, and a reexamination of the analytical approach, better constrained by recent data, was necessary. The larger incident energy domain used here required some energy dependence to be introduced in the parametrization following the general features described above as (loose) guidelines.

In this study, the $\bar{p}$ inclusive cross section will be expressed as a function of the three variables $\sqrt{s}$, $p_\perp$, and x_R (see, for example, [7] for the relevance of the choice of these variables),

$$\frac{E d^3\sigma}{dp^3} = f(\sqrt{s}, p_\perp, x_R). \tag{3}$$

The following functional form used to describe the $\bar{p}$ production cross section is an evolved version of the KMN formula:

$$E\frac{d^3\sigma}{dp^3} = \sigma_{in} A^{C_1 \ln(\sqrt{s}/C_2) p_\perp} (1-x_R)^{C_3 \ln(\sqrt{s})} e^{-C_4 x_R} \times [C_5(\sqrt{s})^{C_6} e^{-C_7 p_\perp} + C_8(\sqrt{s})^{C_9} e^{-C_{10} p_\perp^2}] \tag{4}$$

where A is the target mass. The total inelastic cross section σ_{in} for *pA* collisions was borrowed from [15],

$$\sigma_{in}(\text{mb}) = \sigma_0[1 - 0.62 \exp(-E_{inc}/200)\sin(10.9 E_{inc}^{-0.28})]$$

$$\sigma_0(\text{mb}) = 45 A^{0.7}[1 + 0.016 \sin(5.3 - 2.63 \ln A)] \tag{5}$$

where E_{inc} is the incident kinetic energy in MeV.

The 10 parameters C_1–C_{10} have been fitted to the set of experimental data listed in Table I by a standard χ^2 minimization procedure using the code MINUIT [16].

In relation (4), the term $(1-x_R)^{C_3}$ originates from the hadronic scaling properties, namely the quark counting rules of the parton model of hadronic interactions [8] (see Sec. II). It was found empirically in this study that a significantly better result is obtain if the exponent is energy-dependent. The $\ln(\sqrt{s})$ factor multiplying the C_3 coefficient was found to give the best result. The term $e^{-C_4 x_R}$ is induced by the Regge regime [8]. The last factor of relation (4) accounts for the transverse momentum dependence of the cross section (see Sec. II). The analysis of the experimental data (Table I) showed that the term of angular dependence $e^{-C_{10} p_\perp^2}$ is dominant at low energy, $E_p^{lab} \approx 10$ GeV, while the term

TABLE IV. Antiproton production cross-section data not taken into account in the χ^2 minimization procedure, classified by increasing energy. See text for explanations.

Experience	Target	p_{inc}/E_{inc} (GeV/c)	$\bar{p}$ kinematic range (GeV/c)	θ_{lab} (mrad)
Antipov *et al.* IHEP 1971 [32]	Al	70	p_{lab}: 10–60	0
Abramov *et al.* IHEP 1984 [33]	C, Al, Cu, Sn, Pb	70	$p_\perp$: 0.99–4.65	160
Bozzoli *et al.* CERN 1978 [34]	Be, Al, Pb	200	p_{lab}: 20–37	0
Bearden *et al.* CERN 1998 [35]	Be, S, Pb	450	p_{lab}: 4–8.5 $p_\perp$: 0.11–1.28	37, 131

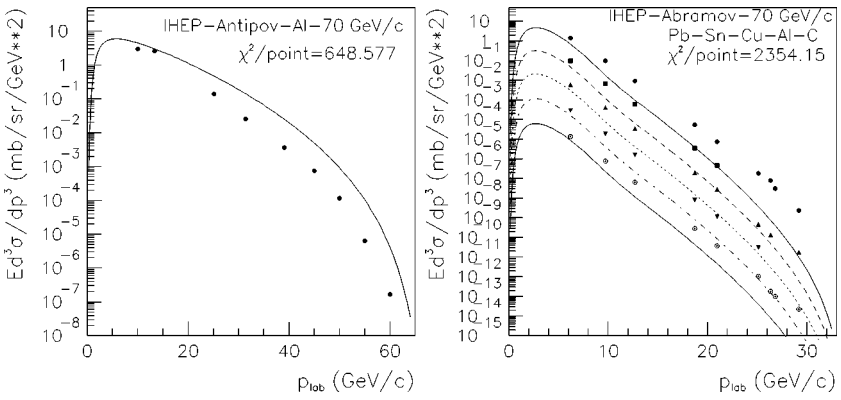

FIG. 7. Experimental data points from [32,33] compared to the best-fit calculations. Data points not included in the final search procedure.

$e^{-C_7 p_\perp}$ dominates at high energies, $E_p^{lab} > 100$ GeV. The $\sqrt{s}$ dependence has been introduced to allow the transition from the $p_\perp$ to the $p_\perp^2$ dependence. The target mass dependence was accounted for by the factor $A^{C_1 \ln(\sqrt{s}/C_2) p_\perp}$, with an energy-dependent exponent introduced for the same reason as above, at variance with the constant exponent used in the KMN parametrization. The energy dependence used (linear in $\sqrt{s}$) accounts for the experimental increase of this coefficient with the incident energy found using the KMN approach. For incident energies $E_p^{lab} < 55$ GeV, this coefficient becomes negative.

In Sec. II, it was mentioned that one of the features of the inclusive distribution is its symmetry in the rapidity space. By construction, our parametrization [relation (4)] satisfies this symmetry property since it depends only on $\sqrt{s}$, $p_\perp$, and x_R. This is illustrated in Fig. 1, which shows the fit to the 23.1 GeV/c cross-section data versus particle rapidity (right) and particle momentum (left). The maximum of the cross section corresponds to particle production with velocity zero in the c.m. frame, i.e., traveling with the c.m. velocity in the laboratory. The corresponding value of this momentum in the laboratory is $p_0 \approx \sqrt{m_p E_p/2}$. Since the cross-section distribution is symmetric in the rapidity space, the upper branch of rapidity with respect to the $y_{\text{c.m.}}$ completely determines the values of the cross section along the lower branch. This is true as well in the laboratory frame, where the values of the cross section for $p > p_0$ determine the values below this momentum. In the case of the figure, this means that a fit to the experimental values of the cross section above $p_0 \approx 3.3$ GeV/c also determines the values of the cross section below with the same level of accuracy. Fitting the data from about $y_{lab} \sim 2.1$ up to $y_{lab} \sim 3.2$ also determines the cross section down to $y_{lab} \sim 0.65$, i.e., down to $p_{lab} \sim 0.65$ GeV/c, the validity of the fit extending likely signifi-

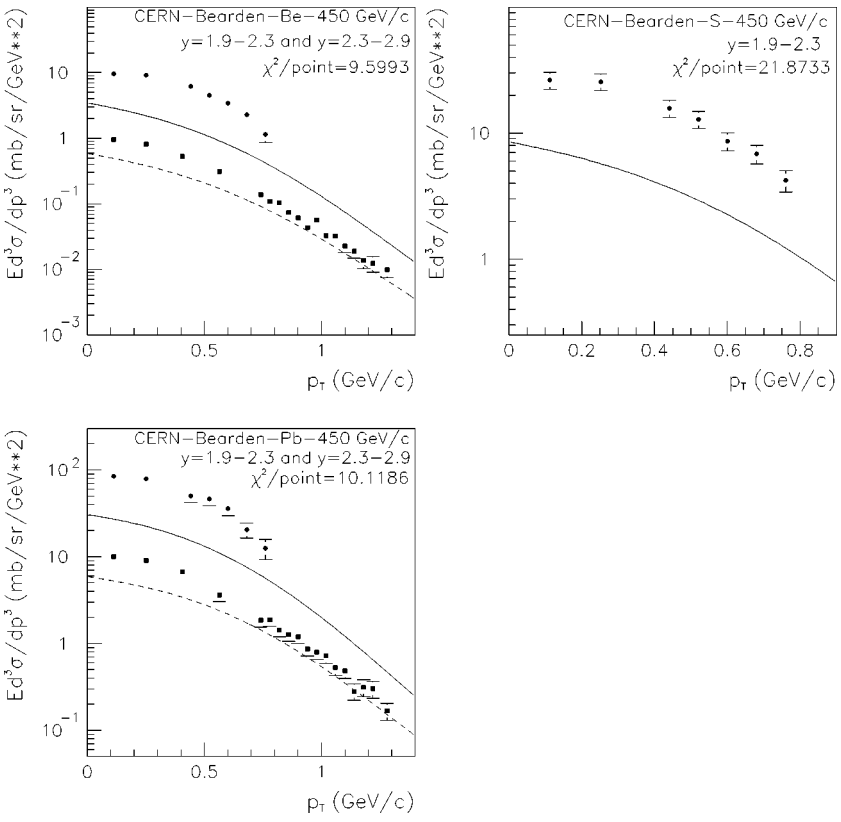

FIG. 8. Experimental data points from [35] compared to the best-fit calculations. Data points not included in the final search procedure.

TABLE V. Values of the parameters of relation (6) obtained by fitting the experimental $\bar{p}$ production cross sections listed in Table III for proton-proton collisions and the corresponding error following the PDG standard conventions.

Parameter	D_1	D_2	D_3	D_4	D_5	D_6	D_7
Value (error)	3.4610(20)	4.340(20)	0.007 855(3)	0.5121(27)	3.6620(5)	0.023 070(1)	3.2540(77)

cantly below this value (within the approximation discussed previously). This is an important point since experimental $\bar{p}$ cross-section data are usually scarce below about 1 GeV, and since the production cross section for these low-energy particles is very important because $\bar{p}$'s originating from neutralino (dark-matter) annihilation [1] or from the evaporation of primordial black holes [2] are expected within this energy range.

IV. RESULTS FOR NUCLEAR TARGETS

The data used in the fit procedure are summarized in Table I. The fit sample included measurements from 12 GeV up to 400 GeV incident proton laboratory energy on nuclear targets going from deuterium up to Pb nuclei, and for momentum transfers up to 6.91 GeV/c. For pp collisions, the incident c.m. energy $\sqrt{s}$ extended from about 6 up to 63 GeV.

The χ^2 per point obtained with the parametrized relation (4) is 5.32 (Table III) for 654 experimental points (see list in Table I). The values of the parameters obtained in the fit are given in Table II together with error. The correlation coefficients between the parameters determined in the search are given in the appendix. The results for nuclear targets ($A \geqslant 2$) are shown in Figs. 2–6, where the data points are compared with the calculated values that are given in the Appendix. The values of the χ^2 per point of each set are given in the figures. In each case, some basic information (authors, beam energy, target nuclei, and χ^2 per point obtained for the considered set) is given in the figures. In all the figures, the top distribution corresponds to the measured cross section, while each next distribution below has been multiplied by a 10^{-1} factor with respect to the previous one, for the legibility of the figure.

As can be seen in the figures, the quality of the fits varies from fair to excellent. A poor fit is obtained, however, for the 24–26 GeV data from [23], the calculations underestimating the data by a factor of about 2. Nevertheless, this set has been kept in the fit procedure since its contribution is small and it hardly affects the results (which is not the case for the data listed in Table IV). On the contrary, outstandingly good fits have been obtained consistently and simultaneously for the CERN data from [20,22] in the 20–25 GeV incident energy range, and for the high-energy and large momentum transfer data from [28,29].

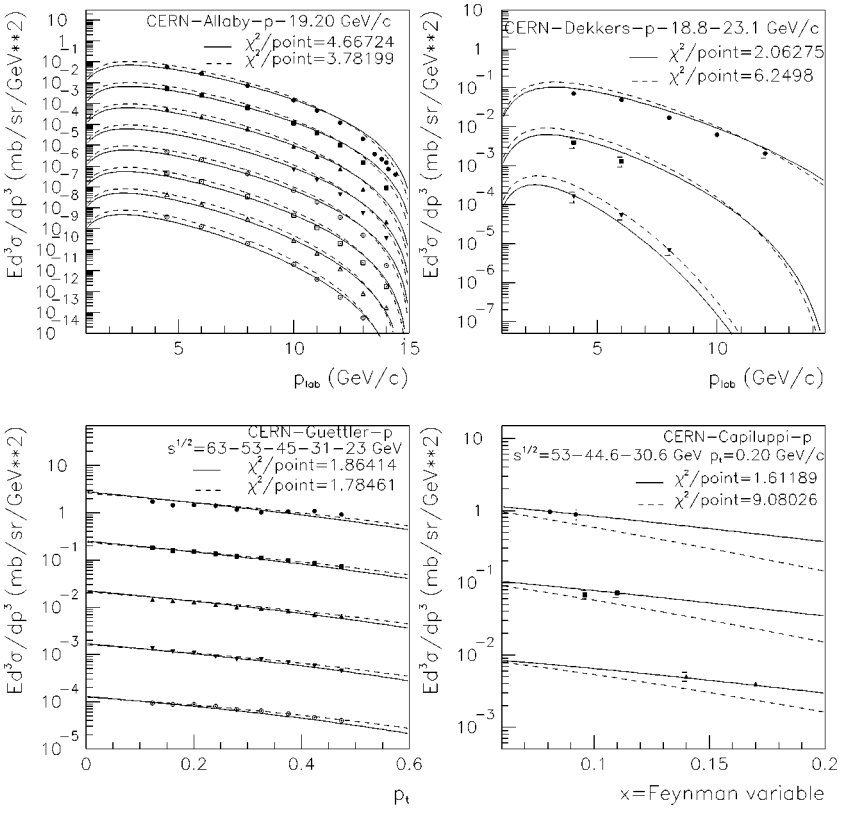

FIG. 9. Experimental data points from pp collisions from [20,21,30,31] compared to the best-fit calculations using the two parametrizations. See text.

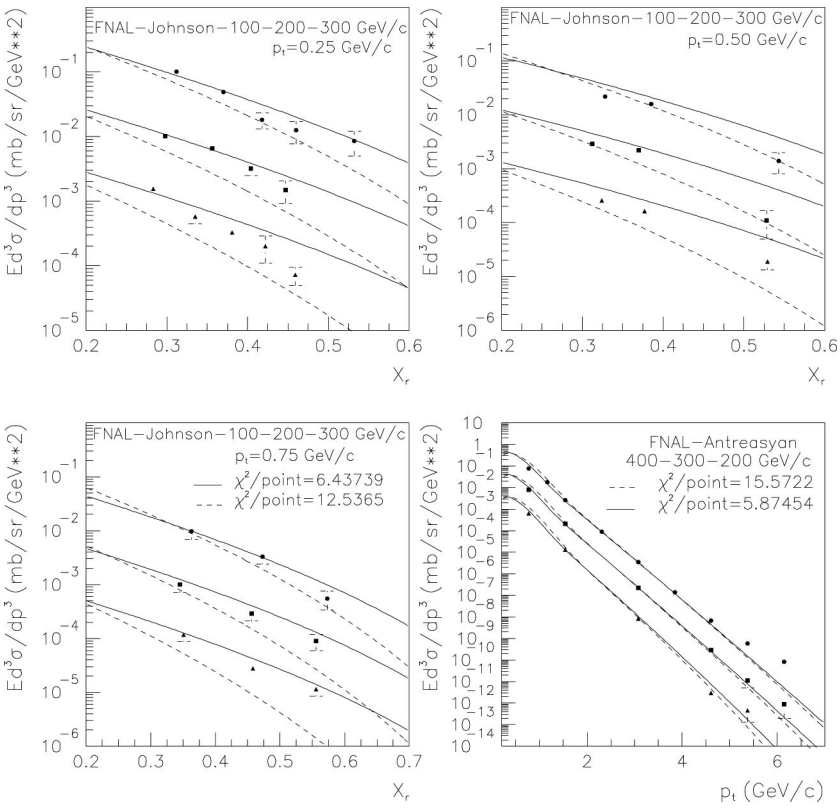

FIG. 10. Same as Fig. 9 for the data from [26,29]. The χ^2 per point for the first three graphs is indicated in graph 3.

Table III compares the values of the χ^2 per point obtained in the present study with that obtained using the KMN relation [3] for the same data. The latter is seen to be more than one order of magnitude larger than the value obtained using Eq. (4). This gives the scale of the improvements achieved by the present study on the issue.

These results demonstrate the ability of the proposed parametrization to describe the inclusive $\bar{p}$ production cross section on nuclei over the quoted ranges of incident energy, momentum transfer, and target mass, with good accuracy.

A. Data discarded from the selection

The data listed in Table IV were not included in the fit sample because of their obvious inconsistency with the other data. This is illustrated in Figs. 7 and 8, where they are compared to the best-fit calculations obtained in the previous step on the selected sample. As can be seen, the difference between data and calculated values amounts up to about one order of magnitude. The ratio goes from 2 to 10 for the Serpukhov experiments [32,33]. For [32], it is about 5, consistent with a simple normalization problem.

A larger and more surprising disagreement is found with some recent CERN data from NA44 [35], in particular for the measurements in the small rapidity bin. Note also that the parametrization (6) describes quite well the data from [29] obtained on the same targets as [35] over a wider kinematic region (see Fig. 6).

The $\bar{p}$ cross-section data from [34] appearing in the table were given in the original works in units of the corresponding π^- production cross section measured at the same momentum. Although the absolute value could be obtained using the known π^- cross section, the results were considered too inaccurate, however, and discarded from the selected sample.

B. Analysis of the $pp \to \bar{p}X$ data

This reaction is the dominant contribution to the secondary $\bar{p}$ production induced by cosmic rays, since the interstellar gas is mainly constituted of hydrogen gas. It is thus important to obtain as accurate a description as possible for the cross section.

Considering separately the $p+p$ collision data in Table I, the parametrization (4) gives for the best fit a value of the χ^2 per point of 7.08. For the same data, the well known parametrization of Tan and Ng [36] gives a value of 28.1. In addition, this latter parametrization is valid only for $p_\perp = 0 - 0.8$ GeV/c and is not able to reproduce the large $p_\perp$ data such as those from [28] and [29] where $p_\perp = 0.76 - 6.91$ GeV/c. Note also that Tan and Ng's parametrization contains eight parameters for $\sqrt{s} > 10$ GeV ($p_{lab} > 50$ GeV/c) and 17 for $\sqrt{s} < 10$ GeV.

However, in the course of the study, it appeared that some of the parameters of relation (4) had no incidence on the resulting fits. The parametrization (4) has then been revisited and simplified from some of its parameters that are irrelevant for this particular reaction and from other parameters which turned out to be ineffective in the minimization procedure, resulting in the following functional form for the $pp \to \bar{p}X$

inclusive production cross section:

$$E\frac{d^3\sigma}{dp^3}=\sigma_{in}(1-x_R)^{D_1}e^{-D_2x_R}$$
$$\times[D_3(\sqrt{s})^{D_4}e^{-D_5p_\perp}+D_6e^{-D_7p_\perp^2}]. \quad (6)$$

In comparison with relation (4), the dependence with the mass of the target has been removed since only the proton target is considered in this case. In addition, the energy-dependent factors $\sqrt{s}$ in front of D_1 and D_7 in Eq. (4) have also been removed because of their ineffectiveness in the minimization procedure.

The parameters D_1 to D_7 have been adjusted by the same χ^2 minimization procedure as previously [16] to the set of experimental data listed in Table I restricted to *pp* collisions. With formula (6), the χ^2 per point obtained for the best fit is 3.59 for 228 experimental points instead of 7.08 with relation (4). The values of the fit parameters obtained with Eq. (6) are given in Table V. The correlation coefficients between the parameters determined in the search are given in the Appendix. Note that the values of the coefficients C_3 and D_2, and C_5 and D_3, respectively, are of the same order of magnitude. This was expected since they describe the same physics in the relations (4) and (6).

Figures 9 and 10 show the $pp\rightarrow\overline{p}X$ data analyzed compared with the best-fit results obtained for the whole *pp* and *pA* data sets from Table I using relation (4) (dashed line), and with those obtained for the *pp* data only using relation (6) (solid line). The simplified form (6) clearly provides a significantly better account of the measured cross sections, the χ^2 value obtained being better by a factor of about 2 (about 3.6 against about 7).

The results obtained in this work have been used in the calculations of the $\overline{d}$, $\overline{t}$, and $\overline{\mathrm{He}}$ production from $p+p$ and $p+A$ collisions in the atmosphere and in the galaxy [37–39].

V. ANTIPROTON MEAN MULTIPLICITY

In this section, the antiproton mean multiplicity, defined as

$$\langle n_{\overline{p}}\rangle=\frac{1}{\sigma_{in}}\int f\frac{d^3p}{E}, \quad (7)$$

and depending only on $\sqrt{s}$, has been computed by means of relations (4) and (6) and compared with the experimental data in the *pp* collision [40]. Note that the original data from [40] have been corrected from the single-diffractive contribution to the total inelastic cross section σ_{in} [41]. The corrected antiproton mean multiplicity should thus be somewhat smaller than the measured values (by $\sim$15–20 %).

The results, shown in Fig. 11, are in good agreement with the experimental data. Note that below $\sqrt{s}\simeq 15$ GeV/c, the results given by the relations (4) and (6) become significantly different (about a factor 2 at the maximum). As expected, the simplified form (6) gives a little bit better results since the experimental data are from *pp* collisions.

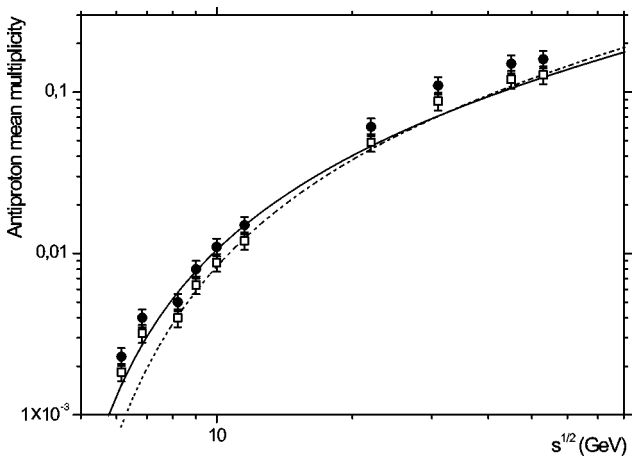

FIG. 11. Antiproton mean multiplicity distribution in the whole phase space, calculated using relation (4) (solid line) and relation (6) (dashed line), compared with experimental data [40], uncorrected (full circles) and corrected (open squares) from diffractive contribution. See text for details.

VI. CONCLUSION

The parametrization of the $\overline{p}$ inclusive production cross section on nuclei has been reexamined by investigating a broad collection of data sets available, covering a large dynamical domain of incident energy and of momentum transfer, for a broad range of nuclear masses. Good results have been obtained but for a small sample of data sets inconsistent with the other data. The experimental $\overline{p}$ inclusive production cross sections can be reproduced to within a few tens of percent over this range, i.e., for incident energies from 12 GeV up to 400 GeV, and for target mass $1\leqslant A\leqslant 208$. These results constitute a significant improvement with respect to the former KMN parametrization, decreasing by a factor of about 15 the value of the χ^2 per point obtained using the latter. A simplified version of the functional form has been developed for *pp* collisions giving also good results up to very high energies, much beyond the range dictated by the cosmic ray physics requirements which motivated the study. This also constitutes an improvement, consistent with the data on nuclei, of the Tan and Ng formula used so far as a standard in the calculations.

The parametrizations (4) and (6) are also able to reproduce the experimental antiproton mean multiplicity measured in *pp* collision with a good accuracy.

A point to be emphasized is that because of the symmetry of the cross section in the rapidity space, the fitted range in the laboratory momentum of the particle, usually measured above the c.m. rapidity, also determines the cross section at low momenta, a range of major importance for cosmic ray antiprotons where accuracy is extremely important.

ACKNOWLEDGMENTS

The authors are grateful to Michael Murray for helpful discussions on the NA44 data.

APPENDIX

The symmetrical matrices (A1) and (A2) give, respectively, the correlation coefficients for the parameters C_1-C_{10} and D_1-D_7 of Eqs. (4) and (6), respectively.

In relation (4), the coefficients C_1 and C_2 appear to be strongly correlated (correlation coefficient 0.961), as could be expected from their functional dependence. On the contrary, coefficients C_5 and C_8 are not correlated (correlation co-efficient 0.232), since they are effective in different energy ranges (see Sec. III). The same remarks apply to the co-efficients D_1-D_7.

The correlation coefficients for the parameters C_1-C_{10} given in Table II are

$$\begin{pmatrix} 1.000 & 0.961 & 0.120 & -0.200 & -0.148 & 0.128 & 0.086 & -0.067 & -0.048 & -0.165 \\ & 1.000 & 0.131 & -0.209 & -0.199 & 0.157 & -0.098 & -0.067 & -0.060 & -0.148 \\ & & 1.000 & -0.937 & -0.321 & 0.228 & -0.049 & -0.655 & -0.620 & -0.289 \\ & & & 1.000 & 0.282 & -0.180 & -0.042 & 0.834 & 0.784 & 0.311 \\ & & & & 1.000 & -0.962 & 0.358 & -0.110 & -0.128 & 0.239 \\ & & & & & 1.000 & -0.164 & 0.232 & 0.286 & -0.202 \\ & & & & & & 1.000 & -0.127 & 0.007 & -0.028 \\ & & & & & & & 1.000 & 0.979 & 0.210 \\ & & & & & & & & 1.000 & 0.148 \\ & & & & & & & & & 1.000 \end{pmatrix} \tag{A1}$$

The correlation coefficients for the parameters D_1-D_7 given in Table V are

$$\begin{pmatrix} 1.000 & -0.933 & -0.557 & 0.604 & 0.080 & -0.311 & 0.087 \\ & 1.000 & 0.654 & -0.730 & -0.141 & 0.435 & -0.135 \\ & & 1.000 & -0.979 & 0.502 & -0.212 & -0.241 \\ & & & 1.000 & -0.336 & 0.033 & 0.228 \\ & & & & 1.000 & -0.833 & -0.213 \\ & & & & & 1.000 & 0.282 \\ & & & & & & 1.000 \end{pmatrix}. \tag{A2}$$

[1] See, for example, G. Jungman *et al.*, Phys. Rev. D **49**, 2316 (1994).
[2] A. Barrau *et al.*, Astron. Astrophys. **288**, 676 (2002).
[3] A.N. Kalinovskii, M.V. Mokhov, and Yu.P. Nikitin, *Passage of High-energy Particles through Matter* (American Institute of Physics, New York, 1989).
[4] C.Y. Huang and M. Buénerd, Report ISN-01-18, March, 2001; C.Y. Huang, Ph.D. thesis, University of Grenoble, 2002.
[5] C.Y. Huang, L. Derome, and M. Buénerd, Phys. Rev. D **68**, 053008 (2003).
[6] E. Byckling and K. Kajantie, *Particle Kinematics* (Wiley Interscience, London, 1973).
[7] F.E. Taylor *et al.*, Phys. Rev. D **14**, 1217 (1976).
[8] P.D.B. Collins and A.D. Martin, *Hadron Interaction* (Adam Hilger Ltd, Bristol, 1984).
[9] D. Horn and F. Zachariasen, *Hadron Physics at Very High Energy* (W.A. Benjamin, Inc., Advances Book Program, Massachusetts, 1973).
[10] T. Abbott *et al.*, Phys. Rev. D **45**, 3906 (1992).
[11] M. Aoki *et al.*, Phys. Rev. Lett. **69**, 2345 (1992).
[12] A. Bussière *et al.*, Nucl. Phys. **B174**, 1 (1980).
[13] T. Abbott *et al.*, Phys. Rev. C **50**, 1024 (1994).
[14] A. Jahns *et al.*, Phys. Rev. Lett. **68**, 2895 (1992).
[15] J.R. Letaw *et al.*, Astropart. J. Suppl. Ser. **51**, 271 (1983).
[16] F. James, MINUIT, Fonction Minimisation and Errore Analysis, CERN, Program Library Long Writeup D506, 1998.
[17] Y. Sugaya *et al.*, Nucl. Phys. **A634**, 115 (1998).
[18] G.J. Marmer *et al.*, Phys. Rev. **179**, 1294 (1969).
[19] T. Abott *et al.*, Phys. Rev. C **47**, R1351 (1993).
[20] J.V. Allaby *et al.*, CERN-70-12 Nuclear Physics Division (1970).
[21] D. Dekker *et al.*, Phys. Rev. **51**, 271 (1965).
[22] T. Eichten *et al.*, Nucl. Phys. **B44**, 333 (1972).
[23] P.I.P. Kalmus *et al.*, CERN-71-25 Nuclear Physics Division (1971).
[24] J.M. Snow *et al.*, Phys. Rev. D **32**, 11 (1985).
[25] D.S. Barton *et al.*, Phys. Rev. D **27**, 2580 (1983).
[26] J.R. Johnson *et al.*, Phys. Rev. D **17**, 1292 (1978).
[27] W.F. Baker *et al.*, Phys. Lett. **51B**, 303 (1974).
[28] J.W. Cronin *et al.*, Phys. Rev. D **11**, 3105 (1975).

[29] D. Antreasyan *et al.*, Phys. Rev. D **19**, 764 (1979).
[30] K. Guettler *et al.*, Nucl. Phys. **B116**, 77 (1976).
[31] P. Capiluppi *et al.*, Nucl. Phys. **B79**, 189 (1974).
[32] Yu.M. Antipov *et al.*, Phys. Lett. **34B**, 164 (1971).
[33] V.V. Abramov *et al.*, Z. Phys. C **24**, 205 (1984).
[34] W. Bozzoli *et al.*, Nucl. Phys. **B144**, 317 (1978).
[35] I.G. Bearden *et al.*, Phys. Rev. C **57**, 837 (1998).
[36] L.C. Tan and L.K. Ng *et al.*, Phys. Rev. D **26**, 1179 (1982).
[37] R.P. Duperray, K.V. Protasov, and A.Yu. Voronin, Eur. Phys. J. A **16**, 27 (2003).
[38] R.P. Duperray, K.V. Protasov, L. Derome, and M. Buénerd, Eur. Phys. J. A (to be published), nucl-th/0301103.
[39] B. Baret *et al.*, ICRC2003 Conf. Proc., Tsukuba (Japan), 2003.
[40] M. Antinucci *et al.*, Lett. Nuovo Cimento Soc. Ital. Fis. **6**, 121 (1973).
[41] G. Giacomelli *et al.*, Nuovo Cimento Soc. Ital. Fis., C **24C**, 575 (2001).